Hindawi
International Journal of Polymer Science
Volume 2019, Article ID 6194674, 15 pages
https://doi.org/10.1155/2019/6194674

Review Article

Understanding Collaborative Effects between the Polymer Gel Structure and the Applied Electrical Field in Gel Electrophoresis Separation

Jennifer A. Pascal,[1] Koteswara Rao Medidhi,[1] Mario A. Oyanader,[2] Holly A. Stretz,[1] and Pedro E. Arce[1]

[1]*Department of Chemical Engineering, Tennessee Technological University, Cookeville, TN 38505, USA*
[2]*Department of Chemical Engineering, California Baptist University, 8432 Magnolia Ave, Riverside, CA 92504, USA*

Correspondence should be addressed to Pedro E. Arce; parce@tntech.edu

Received 24 July 2018; Accepted 9 January 2019; Published 17 April 2019

Academic Editor: Bernabé L. Rivas

The collaborative effects between an applied orthogonal electrical field and the internal structure of polymer gels in gel electrophoresis is studied by using microscopic-based electrophoretic transport models that then are upscaled via the format of electro kinetics-hydrodynamics (EKHD). The interplay of the electrical field and internal gel morphology could impact the separation of biomolecules that, because of similar chemical properties, are usually difficult to separate. In this study, we focus on an irregular pore geometry of the polymer-gel structure by using an axially varying pore (i.e., an axially divergent section) and an orthogonal (to the main flow of solutes) applied electrical field. The microscopic-based conservation of species equation is formulated for the standard case of electrophoresis of charged particles within a geometrical domain, i.e., a pore, and upscaled to obtain macroscopic-based diffusion and mobility coefficients. These coefficients are then used in the calculation of the optimal time of separation to study the effect of the varying parameters of the pore structure under different values of the electrical field. The results are qualitatively consistent with those reported, in the literature, by using computational-based approaches as well as with experiments also reported in the literature, previously. The study shows the important collaborative effects between the applied electrical field and the internal geometry of the polymer gels that could lead to improving biomolecule separation in gel electrophoresis.

1. Introduction, Motivation, and Previous Efforts

The separation of biomacromolecules can be accomplished in various types of porous/fibrous media with electrophoresis, including polymer gels, microfluidic and field flow fractionation devices, and capillary electrophoresis, just to name a few [1–3]. Separation of these molecules has many potential applications, including the development of new pharmaceuticals, tissue scaffolding, and clinical diagnostic tests [4, 5]. In spite of excellent advances made among many of the electro-driven separation techniques, gel electrophoresis and its variations (2D gel electrophoresis, SDS-PAGE electrophoresis, temperature gradient gel electrophoresis, etc.) remains the widest used separation technique for proteomics, DNA/RNA fragments, and other macromolecules and it is a multimillion dollar business (Apogee Electrophoresis, 2014). Therefore, improvements in the separation efficiency will have a highly beneficial impact on the technology.

The use of an orthogonal field in gel electrophoresis can improve the separation of biomolecules. In particular, when the physicochemical properties of these biomolecules are similar and the separation can become very challenging, the presence of an orthogonal field is helpful. Sauer et al. [6] were the first contribution to explain the beneficial role of orthogonal fields found in experimental trends [7], from fundamental principles. Oyanader and Arce et al. [8] further identified the role of geometrical scales of the gel pore matrix in

controlling the separation and, in addition, determining optimal time of separations. Pascal et al. [3] extended the analysis to electro-field flow fractionation in Couette-type separation devices.

In addition to the applied electrical field, another key aspect controlling the separation efficiency in electrophoresis is the internal structure, or morphology, of the gel media. Since gels are polymer matrices with pores of different sizes, shapes, and geometries and that only one of these is not enough to capture the separation behavior of the system [9, 10], it is important to gain a deeper understanding of the role that the gel pore geometry can play on the electrophoresis separation efficiency of macromolecules and their optimal time of separation. Early successful studies reported explained the potential impact of the geometry of the pores in the gel morphology, on electrophoresis separation, and included the use of a sudden change in the axial direction of the cross-sectional area of a pore domain of a gel medium [11]. Furthermore, a Monte Carlo simulation approach was used in either an isotropic or a nonisotropic gel morphology [12, 13] to determine the effective diffusivity of "point molecules" inside a model gel matrix. All of these studies show the crucial role that the pore-gel morphology could play in dictating the values of the effective transport parameters of biomolecules that, in turn, control their optimal time of separations.

As opposed to a sudden change in the cross-sectional area of flow in the gel-pore domain [11], Simhadri et al. [14] reported a computational analysis based on pores of rectangular geometry with an axially varying cross section. The current contribution examines the role of the same pore geometry, also with a rectangular diverging pore from an analytical point of view, i.e., *a continuously axially varying cross section* of the gel-pore domain (linear fashion) and its effect on the prediction of optimal separation times coupled with an orthogonal applied electrical field (constant). Through the use of the methodology known as "electrokinetic hydrodynamics," or EKHD [15, 16], the relevant physics of the motion of the biomolecule inside the gel matrix is captured based on microscopic differential models of the gel-pore domain. Then, the model is upscaled to the macropore level by using the spatial-averaging method, a scaling technique, in conjunction with the fundamental principles of electrostatics and hydrodynamics. This approach is useful in obtaining the effective diffusivity and the effective mobility of the biomolecule (inside the gel matrix); then, these effective coefficients are used to compute optimal separation times as well as to assess the role of the axially varying morphology of the pore domain of the gel matrix on its separation performance. This can be accomplished by varying the various geometrical parameters of the diverging section, i.e., aspect ratio, angle of divergence, and axial position, and illustrating their impact on both the effective transport parameters as well as the optimal separation time as functions of the applied electrical field. One of the advantages of using the EKHD approach is that the universal or generalized dispersion coefficients (see Section 4) as well as the optimal separation time are *explicit functions* of the geometrical parameters controlling/affecting the morphology of the pore domain of the gel matrix and the applied orthogonal electrical field. This is an advantage with respect to computational simulations [14] where the relation of the effective transport coefficients, with geometrical parameters of the pore domain, is not explicit.

This study shows the important interplay among model scaling, pore morphology of the gel matrix, charge of the biomolecule, and the applied orthogonal electrical field in assessing or improving electrophoresis separations. In addition, the optimal times of separation that are obtained are relatively simple mathematical functions, and therefore, they lead to a tunable model that can predict behaviors of the system performance for a wide range of variables (i.e., magnitude of the applied orthogonal electrical field, angle of divergence, aspect ratio, axial position, etc.). The effects of these geometrical parameters as well as the molecule charges and the magnitude of the applied orthogonal electrical field on the optimal separation time are illustrated. Furthermore, a qualitative agreement between the predictions reported here with those published by Simhadri et al. [14] is observed. Both predictions (those communicated here and those by Simhadri et al. [14]) are in agreement with experimental evidences reported by Thompson et al. [17].

This contribution is organized as follows. First, a detailed introduction and reference to previous work on the subject is given in Section 1. Next, an overview of the related literature and remarks where this contribution differentiates from others is presented in Section 2. The formulation of the so-called fluid problem [15, 16] is introduced in Section 3 and its subsections on electrostatics and hydrodynamic aspects. The "solute problem" equations are developed in Section 4, and the upscaling of the model is performed here leading to the effective diffusivity and effective mobility. Asymptotic solutions and validation are discussed in Section 5. Parametric illustrations and discussions of results are presented in Section 6. Section 7 is a discussion of the implications of the finding for the practical aspects of the problems; in particular, calculations of the optimal time of separation and the effect of the different parameters are included. Finally, concluding remarks are given in Section 8 of the study.

2. Overview of Relevant Literature

Biomacromolecules, in general, can often have similar physical or transport properties, i.e., electrophoretic mobility and/or diffusivity, causing the separation to become very challenging in certain cases [18]. In addition to the applied electrical field, for a given mixture of biomacromolecules, the internal gel structure, or morphology of the gel media, is one key property that can be exploited to enhance the separation efficiency of the material or device. Gels for electrophoresis are fibrous or porous matrices that can expose the biomacromolecules to a "differentiating" medium allowing the physical properties of the molecules, i.e., charge, size, shape, etc., to yield a unique motion for biomacromolecules. This unique motion is controlled by two different transport properties, i.e., effective diffusivity and effective mobility of the molecules inside the gel media. There are few experimental techniques that researchers have used to modify the morphology of the gel matrix. The traditional one is to change the

concentration of the polymer cross-linker (see, for a review, Stellwagen [19]). A novel one is to use templating agents both within the polymer-chemical structure (molecular imprinting, see for a review Byrne and Salian [20]) and to manufacture gels by using molecular templates such as DNA and xanthan. For instance, Dharia et al. [21] and Rill et al. [22] proposed a modified architecture or morphology, by templating gels with DNA (or surfactant) templates that were removed from the gels once the polymerization took place, by electrophoresis action. The resulting material morphology, hypothesized as a "dual" porous structure [11, 13, 23, 24] displaying both small (of the order of the interfiber voids) and large (of the order of the templating agent) pores or voids, showed an improved efficiency in the electrophoretic separation of proteins. The most recent approach to modifying the morphology of the separation media is to add nanoparticles of different characteristics, i.e., nanocomposite gels, that could affect the separation efficiency (see, for example Thompson et al. [17, 23]). This subject has been reviewed by Simhadri et al. [25]; see also Texter [26].

Structurally, gel matrices can be viewed as consisting of pores of different geometries, sizes, shapes, etc. This situation leads to the fact that, realistically, only one *idealized geometry*, i.e., rectangular, cylindrical, or annular, for instance, is not enough to capture the internal architecture of the media [9, 10]. Instead, a collection of these may represent different limiting physical situations that can, *collectively*, aid to understanding the transport and separations of biomacromolecules. In addition, and based on the use of relatively simple geometrical models, Trinh et al. [11–13] were able to show that the geometry of the pores or capillary channels could play a significant role in the determination of the effective transport properties of biomacromolecules.

The use of pores or capillary channels with *axially varying cross sections* is not uncommon in studies of transport phenomena. For example, the effect of an axially varying cross section on the transport of solute in a cylindrical capillary was studied by Horner [27] in order to predict the behavior of atherosclerosis in blood vessels. In this study, the lubrication approximation for the hydrodynamics in conjunction with the spatial averaging approach (Cwirko and Carbonell [28]; Paine et al. [29]; Slattery [30]; Whitaker [31]; Zanotti and Carbonell [32–34]) was used in order to obtain both effective transport parameters as well as concentration profiles of the solute within the artery. Xuan et al. [35] further studied, experimentally, the effect of pressure on the movement of polystyrene particles in a converging diverging microchannel. The ratio of the particle velocity in the throat to that in a straight channel was studied in terms of pressure gradient, particle size, and particle trajectory.

Several contributions have been reported in the literature related to the electrokinetic transport in rectangular channels of varying cross section for applications in bioseparations and microfluidics. For instance, Ghosal [36] studied the transport of a polyelectrolyte through a nanopore with variable axial cross section and examined the effects of an (*axially*) applied electrical field. Through the use of electrostatics and hydrodynamics within a continuum mechanics framework, expressions for the electrophoretic speed of the polyelectrolyte, representative of a typical strand of DNA often used in gel electrophoresis, were determined. Four different modes of transport of the polyelectrolyte were found as a function of the dimensionless height of the channel. It was noted that the use of continuum hydrodynamics with water as the buffer is a reasonable approach that is valid for pores of sizes as low as tenths of a nanometer. In addition, Ghosal [37] also examined electroosmotic flow through a microfluidic channel of varying axial cross section and arbitrary zeta potential distribution. Supported by the use of Green's function associated with the problem, a number of asymptotic cases for the electrohydrodynamic profile were studied as a function of the aspect ratio, $\gamma = \mathrm{H/L}$, including cases for the long channel approximation ($\gamma \ll 1$). Although many of these studies are more relevant for electrokinetic-based separations than for electrophoresis, one general conclusion is that the variable axial cross section increases mixing, worsening the resolution for an electro-based separation.

Opposite to the observation made above, Ross [38] examined electrokinetic separations in a diverging microchannel and found, for a specific case, that the diverging channel could actually lead to a better separation than a straight channel could. Yariv and Dorfman [39] studied the electrophoretic transport in rectangular channels of periodically varying cross sections. Macrotransport theory, as described by Brenner and Edwards [1], was used to obtain expressions for the effective velocity and effective dispersion within the channel. The analysis yielded asymptotic results for the macroscopic transport parameters (i.e., effective mobility and effective diffusivity) for both small and large Peclet numbers. Xuan et al. [35] examined the electrophoretic motion and separation of *particles* within a converging-diverging microchannel fabricated with poly(dimethylsiloxane) chips. The dependence of the separation on electrical field strength, particle size, and morphology was studied by using the ratio of the velocity of the particle at the throat of the device to that in a straight microchannel as the main parameter. Ghosal [37] presented an analysis related to channels of varying cross sections; he examined that electroosmotic flow and sophisticated mathematical techniques were employed to obtain volume fluxes for various geometries and zeta potential distributions. In addition, Yariv and Dorfman [39] also computed expressions for dispersion and effective velocity but only for very large and small Peclet number values. None of these contributions, however, have reported any study of the role of the orthogonal electrical fields in conjunction with the characteristics of the pore or the separation domain nor have they shown any calculation of the optimal time of separation.

In this contribution, and for the particular case of gel-based electrophoretic applications, attention is given to the analysis of orthogonal (The word "orthogonal" here implies perpendicular to the axial (varying) direction of the capillary channel as it was used in Oyanader and Arce [8].) applied electric fields to potentially enhance the separation. As mentioned in Section 1, above, Sauer et al. [7] studied this effect on the transport of solute in a Poiseuille flow regime using a capillary channel or pore of rectangular geometry. Before the work reported by Sauer et al. [6], only ad hoc expressions

were known for dispersion under the influence of an applied electrical field (Eringen and Maugin [40]; Hiemenz [41]; Hunter [42]) and the effects of an orthogonal electrical field were only known experimentally (Lee et al. [7]; see also Gajdos and Brenner [43], Heller et al. [44], and Hiemenz [41]). Sauer et al. [6] introduced a mathematically nontrivial and fundamental modeling approach as a tool for the analysis of the system under study. This effort was the first that *systematically* explained experimental trends (Lee et al. [7]) in enhancing separation efficiency when an orthogonal field is applied in electrophoretic separations. One limitation of the analysis is that the predicting formulae for the effective transport parameters are in terms of integrals that require numerical solution. Motivated by this limitation, and attempting to further apply and/or develop the methodology, Oyanader and Arce [8] have revisited this contribution and have derived simpler and mathematically friendlier expressions for the effective transport parameters that clearly show the dependence on the orthogonal electrical field and the scaling. More specifically, Oyanader and Arce [8] have shown that these expressions depend critically on the scaling of the geometrical parameters of the device. The present analysis is concerned with the effect of an applied orthogonal electrical field on a rectangular pore with (continuously) axially varying cross sections. To the best of our knowledge, this is the first analytical-based contribution in this subject. A computational-based approach was reported by Simhadri et al. [14].

In general, the effects of transverse or orthogonal applied electrical fields have not been *extensively* studied regarding the separation of biomacromolecules, except for the case of electro-FFF (see, for example, Pascal et al. [3]). However, Baldessari and Santiago [45] in a review related to electrophoresis in nanochannels stated that the presence of the thick electrical double layer (EDL) in nanochannels can produce transverse electrical fields. Because of this observation, the dispersion in nanochannels must then be a function of the applied orthogonal electrical field. Therefore, in addition to the previous work by Sauer et al. [6] and Oyanader and Arce [8], Baldessari and Santiago's [45] work suggests that further examining the role of applied orthogonal electrical fields in the separation of biomacromolecules in various systems is important.

3. Problem Formulation: General Framework and Methodology

The system under study in this contribution is depicted in Figure 1. This figure is a general representation of the different scales presented in a gel-electrophoresis system. The transport associated with the motion of biomolecules in gel electrophoresis is a multiscale problem: *level 1* (see Figure 1) describes the *macroscopic* scale in the system where in general, pores of different geometries, sizes, shapes, etc., are located at a smaller scale. *Level 2* in the figure shows the pore-scale domain or *microscopic* scale where for example, an axially varying cross-section pore domain can be easily located in the gel matrix. In general, these domains could be oriented in many different ways and have different sizes and shapes. In this contribution, we are interested in a single type of pore orientation with potentially different shapes, all controlled by the so-called "shape factor" ($\gamma = \mathrm{H/L}$). Level 2 is where microscopic transport phenomena based on continuum mechanics can be described. *Level 3* is, therefore, a single-pore domain (representing all the pores of the gel matrix (A distribution of pore orientation can be used to analyze the effect of the microdomain on the macroscale level transport. However, this is beyond the scope of the present work.)) with the Cartesian coordinate system and other important dimensions anchored to the domain.

In level 3 of Figure 1, the pore's geometry is described by Cartesian coordinates with length L and height $H/2$, with a variable axial cross section (i.e., a diverging pore domain), the degree to which is controlled by the angle α. Since the cross section is not uniform, the fluid motion is in both the axial and orthogonal directions; however, only the flow in the axial direction is relevant for the spatial averaging approach used in this study (Cwirko and Carbonell [28]; Paine et al. [29]; Slattery [30]; Whitaker [31]; Zanotti and Carbonell [32–34]). An electrical field is applied in the orthogonal direction (Oyanader and Arce [8]), denoted by the potential, ϕ, on both the upper and lower pore walls. It is also shown in Figure 1 that the walls of the capillary can be mathematically described by the equation of a line, $h(x)$, as follows:

$$h(x) = \tan(\alpha)x + \frac{H}{2}, \tag{1}$$

where $\tan(\alpha)$ is the slope of the line and $H/2$is the y-intercept. Equation (1) above can be expressed in dimensionless form as follows:

$$\widehat{h}(\widehat{x}) = 1 + \frac{2\tan(\alpha)\widehat{x}}{\gamma}, \tag{2}$$

where $\widehat{y} = 2y/H$, $\widehat{x} = x/L$, and $\gamma = H/L$, which is the aspect ratio or "shape factor" of the pore.

The key assumptions for conducting this analysis are as follows: (i) the buffer solution is Newtonian; (ii) the flow is incompressible; (iii) the system is under steady state; (iv) the capillary walls vary slowly (axially) so that the lubrication approximation can be applied to the system (Probstein [4]); (v) no significant charges are present on the walls (i.e., this is an electrophoretic process) and; (vi) there is long channel approximation (The value of γ will be parametrically varied within the range of the approximation.) (γ 1).

The assumptions above will be employed to develop microscopic governing equations for the "fluid problem," i.e., the electrostatics and hydrodynamics of the buffer solution flow, through a systematic approach called "electrokinetic hydrodynamics," or EKHD, that links the two domains in the system under study (i.e., "solute" and "fluid" or buffer domains) ([15, 16]). EKHD emphasizes scaling and involves a series of steps which can be used to obtain upscaled model equations for the electrostatics and hydrodynamics of the system (fluid domain) and by utilizing the spatial averaging technique to connect them with upscaled microscopic

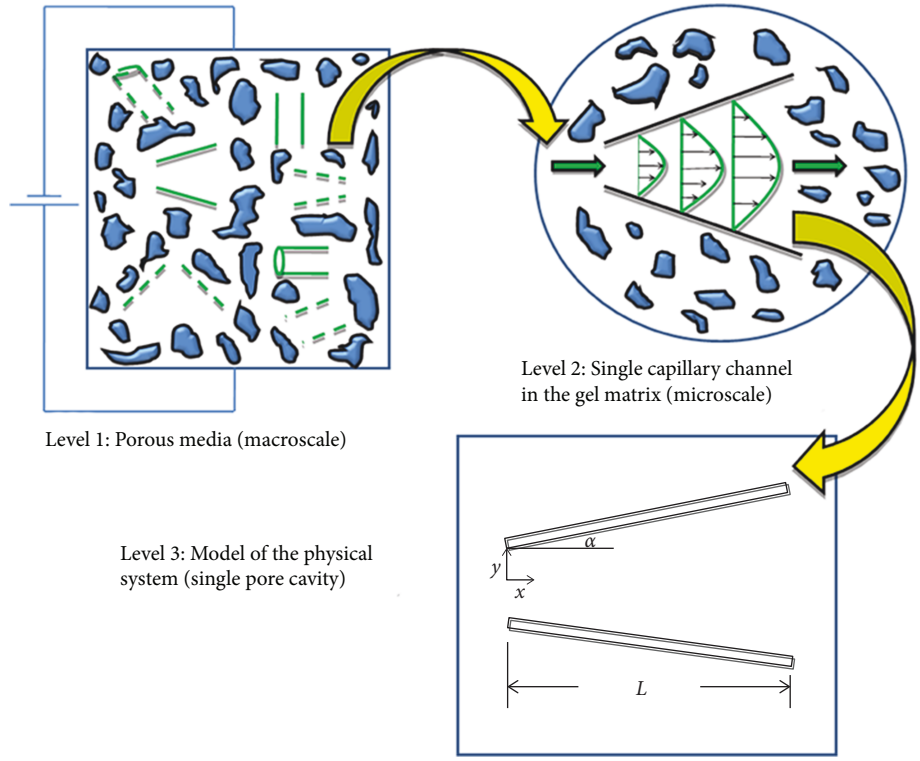

Figure 1: Depiction of the various scales involved in the system under study including a geometrical sketch of the pore and coordinate system used in the analysis.

models such as the species continuity equation (solute domain) (Cwirko and Carbonell [28]; Paine et al. [29]; Slattery [30]; Whitaker [31]; Zanotti and Carbonell [32–34]). From this method, constitutive equations for the effective transport coefficients (i.e., effective mobility and effective diffusivity) can be *analytically* obtained in order to predict the macroscopic or pore-level behavior of the system (A material or gel scale is also possible (see Simhadri [46]); however, in this contribution, we focus only on the pore-level scale. The material scale is equivalent to the "pellet scale" in catalytic systems (see Arce et al. [47]).). These coefficients are a function of fundamental transport parameters, such as the molecular diffusivity, molecular charges, and species electrophoretic mobility. Once these two parameters, i.e., the effective mobility and effective diffusivity, are computed, the optimal separation time for, for example, the two ideal biomacromolecules, or, in general, for a mixture can be determined. This allows for the optimization of the system with respect to the gel morphology shown in Figure 1 (see Simhadri et al. [48]).

In summary, by following the EKHD approach, once the electrostatics and hydrodynamic (formulation and scaling) aspects have been taken care of, and in order to aid in extracting information from the (solute/analyte) species continuity equation (Bird et al. [49]), without actually solving it, the method of spatial (area) averaging is used (Cwirko and Carbonell [28]; Paine et al. [29]; Slattery [30]; Whitaker [31]; Zanotti and Carbonell [32–34]). In particular, this methodology states that any variable of interest, $s(x, y, z)$, can be decomposed into a simple addition of two expressions, i.e., the cross-sectional area average, $\langle s(x, y, z)\rangle$, and a "deviation" function from such an average value, $\tilde{s}(x, y, z)$. Equation (3), below, mathematically expresses this definition while equation (4) further characterizes the mathematical operation needed to obtain the area average of the variable under study:

$$s(x, y, z) = \langle s(x, y, z)\rangle + \tilde{s}(x, y, z), \tag{3}$$

where

$$\langle s(x, y, z)\rangle \equiv \frac{\int_0^W \int_{-\hat{y}(\hat{x})}^{\hat{y}(\hat{x})} s(x, y, z) \cdot dy \cdot dz}{\int_0^W \int_{-\hat{y}(\hat{x})}^{\hat{y}(\hat{x})} dy \cdot dz}, \tag{4}$$

and where $s(x, y, z)$ is any variable of interest such as concentration, velocity, electrical potential, or temperature. It has to be noted that the term $\langle s(x, y, z)\rangle$ is only a function of the axial coordinate "x" and $\tilde{s}(x, y, z)$ remains, in general, as a function of all spatial coordinates of the system, i.e., "x", "y," and "z."

Because the governing equations that describe the fluid domain and solute domain are coupled sequentially, the area-averaging approach on the solute domain can be used to reduce the number of independent variables through an upscaling analysis. In particular, the use of the methodology avoids completely solving the species continuity equation; instead, the approach yields "effective" coefficients that help to predict certain macropore-level performance information (such as the optimal time of separation) as a function of the different conditions of the operating parameters (electrical field strength, divergent angle, pore-domain shape, etc.). In

the sections below, the analysis of the governing equation for the electrical field as well as the coupling between this variable and the species continuity equation are studied. Finally, the use of the spatial area-averaging approach also helps in determining effective transport parameters in "closed-form" mathematical equations that are handy in predicting the behavior of the system performance under a variety of parameter values. This type of analytical equations, for example, cannot be accomplished by other methods such as the Monte Carlo simulation where an algorithmic approach must be used every time that a system parameter is changed (Trinh et al. [12]).

4. Electrostatics

The gel-pore domain depicted in Figure 1 (see level 3) is undergoing electrophoresis; such a domain has an applied electrical field that is governed by the principle of conservation of charges. The pore domain is represented by using Cartesian coordinates. Under the general assumptions typically used in gel electrophoresis [6, 49], the applied electrical field potential for the system shown in Figure 1 is mathematically described by the Laplacian of such an electrical potential.

$$\frac{\partial^2 \Phi}{\partial x^2} + \frac{\partial^2 \Phi}{\partial y^2} = 0, \tag{5}$$

where "Φ" is the applied electrical field potential, "x" is the axial coordinate, and "y" is the orthogonal coordinate to the channel axial direction, x. By neglecting entrance effects as suggested by the analysis described in Oyanader and Arce [8], the orthogonal surface potential, K_2, dominates the variations of the electrical fields, $\Phi(x, y)$, and such a field may be assumed as $\Phi(y)$, explicitly. In addition, Oyanader and Arce [8] showed that for cases where the geometrical ratio satisfies $\gamma \ll 1/7$, equation (5) simplifies for all practical cases to the following (The simplification is typical of an order of magnitude analysis in Laplacian equations describing heat and mass transfer processes as well (see Whitaker [50]).):

$$\frac{\mathrm{d}^2 \Phi}{\mathrm{d}y^2} = 0. \tag{6}$$

Thus, only the orthogonal field direction is important for such a case. Boundary conditions for the orthogonal direction are as follows:

$$\begin{aligned} \Phi\left(y = -\frac{H}{2}\right) &= 0, \\ \Phi\left(y = \frac{H}{2}\right) &= K_2, \end{aligned} \tag{7}$$

where K_2 is the value of the applied electrical potential at the top surface of the pore domain.

In order to study the influence of the electrical field on the system, a solution of equation (6) is needed. Furthermore, this solution must be averaged in the cross section of the capillary to obtain the averaged applied electrical field. This information is needed in the solute transport equation discussed in Section 4, below. Equations (6) & (7) produce the following analytical solution:

$$\Phi(\widehat{x}, \widehat{y}) = \frac{K_2 \widehat{y}}{2\widehat{h}(\widehat{x})} + \frac{K_2}{2}, \tag{8}$$

where $\widehat{y}$, $\widehat{x}$, and $\widehat{h}(\widehat{x})$ are dimensionless variables defined previously. Equation (8) shows that the point, i.e., the "local" applied electrical field potential, $\Phi(\widehat{x}, \widehat{y})$, is a function of both $\widehat{x}$, the dimensionless axial coordinate, and $\widehat{y}$, the dimensionless orthogonal coordinate, due to the axially varying cross section shown in Figure 1. By applying the area-averaging definition (see equation (4)), the area-averaged applied electrical field, $\langle \Phi(\widehat{x}, \widehat{y}) \rangle$, is simply

$$\langle \Phi(\widehat{x}, \widehat{y}) \rangle = \frac{K_2}{2}. \tag{9}$$

The (spatial) area-averaged applied electrical field, $\langle \Phi(\widehat{x}, \widehat{y}) \rangle$, can be related to the point or local potential, $\Phi(\widehat{x}, \widehat{y})$, by the decomposition technique (Gray [2]) to produce

$$\Phi(\widehat{x}, \widehat{y}) = \langle \Phi(\widehat{x}, \widehat{y}) \rangle + \tilde{\Phi}(\widehat{x}, \widehat{y}), \tag{10}$$

where the variable $\tilde{\Phi}(\widehat{x}, \widehat{y})$ is the spatial deviation field defined as

$$\tilde{\Phi}(\widehat{x}, \widehat{y}) = \frac{K_2 \widehat{y}}{2\widehat{h}(\widehat{x})}. \tag{11}$$

In order to predict the effective transport parameters of the system, equations (8), (9), (10), and (11) are useful in solving the species continuity equation as shown in Section 5.

5. Hydrodynamics

The next aspect in studying the convective-diffusive transport of solute/analyte in capillary channels is the hydrodynamics of the buffer solution. As shown in Figure 1, the flow regime under study is laminar- and pressure-driven. Due to the presence of the variable axial cross section, the lubrication approximation becomes useful to obtain an analytical velocity profile. Four requirements, or assumptions, are needed in order to utilize such an approximation. They include that the pressure is a function of the axial coordinate, x, only, the velocity component in the axial direction, x, is a function of y only, and the convective terms in the Navier-Stokes equations are negligible. The first two conditions are a consequence of the long channel approximation, and the last two conditions are a consequence of low Reynolds number flow, as it has been clearly reported in the literature [51, 52]. The following three equations, i.e., the continuity equation and the Navier-Stokes equations for the velocity components in the x- and y-directions, will be

simplified through the lubrication approximation to produce a differential equation for the velocity in the x-direction as a function of the orthogonal coordinate, y.

$$\frac{\partial v_x}{\partial x} + \frac{\partial v_y}{\partial y} = 0, \tag{12}$$

$$\rho\left(v_x \frac{\partial v_x}{\partial x} + v_y \frac{\partial v_x}{\partial y}\right) = -\frac{\partial P}{\partial x} + \mu\left(\frac{\partial^2 v_x}{\partial x^2} + \frac{\partial^2 v_x}{\partial y^2}\right), \tag{13}$$

$$\rho\left(v_x \frac{\partial v_y}{\partial x} + v_y \frac{\partial v_y}{\partial y}\right) = -\frac{\partial P}{\partial y} + \mu\left(\frac{\partial^2 v_y}{\partial x^2} + \frac{\partial^2 v_y}{\partial y^2}\right), \tag{14}$$

where v_x and v_y are velocity in the x- and y-directions, respectively, ρ is the density of the fluid, μ is the viscosity, and P is the pressure. Once the above equations have been identified (Here, the equations are the usual ones for the case of viscous flows since the electrokinetic-based forces are negligible for the buffer solution for the case of *electrophoretic* transport (Arce et al. [53]).), the lubrication approximation can be used and requires defining the following dimensionless variables [51, 52]:

$$\widehat{P} \equiv \frac{P}{\pi}, \tag{15}$$

$$\widehat{v}_x \equiv \frac{v_x}{U}, \tag{16}$$

$$\widehat{v}_y \equiv \frac{v_y}{V}, \tag{17}$$

where π, U, and V are characteristic values for the pressure, velocity in the x-direction, and velocity in the y -direction, respectively. After equations (15), (16), & (17) are substituted into equations (12), (13), and (14), and the assumptions required for the lubrication approximation (stated previously) are employed, the final differential equation for the velocity field in the x-direction as a function of y is shown below. (As previously noted, the effect of the velocity in the y-direction is not relevant for the purposes of this analysis.).

$$\frac{4}{H^2}\frac{\partial^2 v_x}{\partial \widehat{y}^2} = \frac{1}{\mu}\frac{dP(x)}{dx}. \tag{18}$$

Equation (18) has the usual no-slip boundary conditions at each wall, expressed as follows:

$$\begin{aligned} v_x\left(\widehat{y} = \widehat{h}(\widehat{x})\right) &= 0, \\ v_x\left(\widehat{y} = -\widehat{h}(\widehat{x})\right) &= 0. \end{aligned} \tag{19}$$

Equations (18) and (19) produce the following solution for the velocity profile for the system depicted in Figure 1:

$$v_x(\widehat{x}, \widehat{y}) = \frac{H^2}{8\mu}\frac{dP(\widehat{x})}{dx}\left(\widehat{y}^2 - \widehat{h}(\widehat{x})^2\right). \tag{20}$$

Equation (20) is derived under the assumptions that there are no charged walls, the fluid is Newtonian, the flow is incompressible, and the system is under steady-state condition. Next, the pressure gradient as a function of the axial coordinate, x, needs to be determined. This can be accomplished by employing the definition of the volumetric flow rate (Bird [49]):

$$\dot{Q} = \int_A \vec{v} \bullet \vec{n}\, dA. \tag{21}$$

By using equations (20) and (21), the pressure gradient as a function of x can be found in terms of the volumetric flow rate as shown below:

$$\frac{dP(\widehat{x})}{dx} = -\frac{6\dot{Q}\mu}{WH^3\widehat{h}(\widehat{x})^3}. \tag{22}$$

Substituting equation (22) into equation (20) produces the following dimensionless velocity profile for the system shown in Figure 1:

$$\widehat{v}_x = \frac{\widehat{y}^2 - h(\widehat{x})^2}{h(\widehat{x})^3}, \tag{23}$$

where $\widehat{v}_x = v_x/v_{\max}$ and $v_{\max} = 3\dot{Q}/4WH$ is the velocity evaluated at $y = 0$ and $x = 0$.

From equation (23) and by using the spatial area averaging method, as used in the electrostatics section, one can compute the area-averaged velocity for the flow to be

$$\langle \widehat{v}_x(\widehat{x}, \widehat{y}) \rangle = \frac{-2}{3\widehat{h}(\widehat{x})}. \tag{24}$$

The area-averaged hydrodynamic velocity indicated in equation (24) is also a function of the axial coordinate, $\widehat{x}$, as opposed to a constant value in the straight pore domain. Similarly, the deviation equation for the hydrodynamic velocity field is given by

$$\tilde{v}_x(\widehat{x}, \widehat{y}) = \langle \widehat{v}_x(\widehat{x}, \widehat{y}) \rangle \left[\frac{-3\left(\widehat{y}^2 - \widehat{h}(\widehat{x})^2\right)}{2\widehat{h}(\widehat{x})^2} - 1\right]. \tag{25}$$

The above equations will be useful along with the electrostatics equations from Section 3, to study the convective-diffusive transport of solutes in gel-pore domains by performing the spatial averaging, which will be outlined in the next section, below.

6. Convective-Diffusive Molar Transport Equation: Formulation and Analysis

Once the expressions for the area-averaged and deviation of the electrical potential and the hydrodynamic velocity profile of the buffer solution have been computed, as suggested by the EKHD approach [4, 52], it is necessary to link the solute/analyte transport aspects with both the electrostatics (The electrostatics is important in this analysis since the solutes/analytes are charged particles [4]. In particular, it is useful in the computation of the electromigration term of the species continuity equation.) and the hydrodynamics of the buffer solution. This will be accomplished through the use of the spatial averaging approach as applied to the molar species continuity equation as in Sauer et al. [6]. This approach yields expressions for the effective mobility and effective diffusivity which are required for the determination of the optimal separation time, τ_{op}. The steps to obtain these effective parameters are the focus of this section, and the optimal separation time is discussed in detail in Section 6.

The first step in the analysis of the system involves the identification of the species continuity equation on a molar basis as well as the wall boundary conditions associated with such an equation. From Bird et al. [49], the following equation is written for the system under study (see Figure 1, level 3):

$$\frac{\partial C}{\partial t} + v_x(y)\frac{\partial C}{\partial x} = D\left(\frac{\partial^2 C}{\partial x^2} + \frac{\partial^2 C}{\partial y^2}\right) + z\mu\left(\frac{\partial}{\partial y}C\frac{\partial \Phi}{\partial y}\right), \quad (26)$$

where the notation, z, is used to denote the cation valence in a given buffer solution, C is the molar concentration of the species under study, v_x is the axial mass average velocity of the fluid, D is the dilute solution diffusion coefficient of the species, μ is the electrophoretic mobility of the species, and Φ is the applied electrical field potential. Equation (26) has the following boundary conditions at the walls of the channel, implying that the walls are impermeable (Since the spatial area-averaging method is being used, only boundary conditions in the orthogonal direction are specified.):

$$D\frac{\partial C}{\partial y}\Big|_{\tilde{y}=-\tilde{h}(\tilde{x})} + z\mu C\left(-\tilde{h}(\tilde{x})\right)\frac{\partial \Phi}{\partial y}\Big|_{\tilde{y}=-\tilde{h}(\tilde{x})} = 0, \quad (27)$$

$$D\frac{\partial C}{\partial y}\Big|_{\tilde{y}=\tilde{h}(\tilde{x})} + z\mu\left(\tilde{h}(\tilde{x})\right)\frac{\partial \Phi}{\partial y}\Big|_{\tilde{y}=\tilde{h}(\tilde{x})} = 0. \quad (28)$$

By applying the definition of area-averaging to equation (26), the following differential expression is obtained (for details, please see Sauer et al. [6]):

$$\tilde{v}_x(y)\frac{\partial \langle C\rangle}{\partial x} = D\frac{\partial^2 \tilde{C}}{\partial y^2} - z\mu\,\frac{\partial}{\partial y}\left(\langle C\rangle + \tilde{C}\right)\frac{\partial \tilde{\Phi}}{\partial y}. \quad (29)$$

Equation (29) requires the information related to both the deviation function of the velocity profile, $\tilde{v}_x(y)$, and the deviation of the applied electrical field, $\tilde{\Phi}(y)$. These functions were derived in Sections 3 and 4 of this contribution, and they are given by equations (11) and (25), respectively. In addition, equation (29) requires a solution that yields $\tilde{C}(x, y)$ as a function of the spatial area-averaged concentration variable, $\langle C\rangle$. This solution is obtained by using a closure approach such as the one proposed by Cwirko and Carbonell [28] and Paine [29]. Their approach seeks a solution of the following form:

$$\tilde{C}(y) = f(y)\,\langle C\rangle + g(y)\,\frac{\langle v_x\rangle}{D}\,\frac{\partial \langle C\rangle}{\partial x}, \quad (30)$$

where $f(y)$ and $g(y)$ are two algebraic functions of the basic parameters of the system. In the system under study, however, f and g will be implicit functions of the axial coordinate, x, also. In terms of nondimensional variables, $f(\hat{x}, \hat{y})$ and $g(\hat{x}, \hat{y})$ are computed from the differential model and boundary conditions to be

$$f(\hat{x}, \hat{y}) = -1 - \frac{z\Omega e^{z\Omega\hat{y}/2\hat{h}(\hat{x})}}{e^{-(z\Omega/2)} - e^{z\Omega/2}}, \quad (31)$$

$$g(\hat{x}, \hat{y}) = -\frac{2\hat{h}(\hat{x})^2}{z^2\Omega^2} + \frac{48\hat{h}(\hat{x})^2}{z^4\Omega^4} - \frac{\hat{h}(\hat{x})\hat{y}}{z\Omega} + \frac{24\hat{y}\hat{h}(\hat{x})}{z^3\Omega^3} + \frac{6\hat{y}^2}{z^2\Omega^2} + \frac{\hat{y}^3}{\hat{h}(\hat{x})z\Omega} - \frac{48e^{z\Omega\hat{y}/2y\hat{h}\hat{x}})\hat{h}(\hat{x})^2}{z^3\Omega^3\left(-e^{-z\Omega/2} + e^{z\Omega/2}\right)}, \quad (32)$$

where $\Omega \equiv \mu K_2/D$.

Equation (30) is frequently referred to as the "closure" equation of the spatial area-averaging procedure, and in its derivation the assumption of a long capillary, i.e., large value of the geometrical ratio, is used [6, 31]. This is not a restriction in this analysis since the electrical field was computed for a case where $H/L \ll 0.1429$ (Oyanader and Arce [8]). In particular, the nondimensional applied field (Ω) in the orthogonal direction of the flow is the most relevant electrical field parameter of the equation in addition to geometrical dimensions. Based on the spatial/area-average approach [31], the general expressions for the effective transport parameters are given by

$$D_{\text{eff}} = D - \frac{\langle v_x\rangle}{D}\,\langle \tilde{v}_x\, g(\hat{x}, \hat{y})\rangle, \quad (33)$$

$$V_{\text{eff}} = \langle v_x\rangle + \langle \tilde{v}_x f(\hat{x}, \hat{y})\rangle. \quad (34)$$

Furthermore, now equations (33) & (34) can be used to obtain the dimensionless effective parameters, θ and $\hat{V}_{\text{eff}}$, defined as follows:

$$\theta \equiv \frac{1 - D_{\text{eff}}/D}{Pe^2} = \frac{\langle \tilde{v}_x\, g(\hat{x}, \hat{y})\rangle}{\langle \hat{v}_x\rangle H^2}, \quad (35)$$

$$\hat{V}_{\text{eff}} = \frac{V_{\text{eff}}}{\langle v_x\rangle} = 1 + \frac{\langle \tilde{v}_x f(\hat{x}, \hat{y})\rangle}{\langle \hat{v}_x\rangle}, \quad (36)$$

where $\text{Pe} \equiv \langle \hat{v}_x\rangle H/D$ is the Peclet number of the system based on the averaged (axial) velocity as identified in equation (24). The function θ identified in equation (35) is

referred to sometimes as the nondimensional axial dispersion of the capillary and has the advantage of being independent of the Peclet number. In short, it is convenient to view θ as the "universal dispersion" function for every value of the applied orthogonal electrical field since it includes all possible values of the Peclet number as a scaling factor (Mathematically, θ is a self-similar function with Pe, the self-similar parameter of the system. Sometimes, θ is also term as the generalized dispersion coefficient.). Please note that an increase in D_{eff} implies a decrease in θ and vice versa. Both θ and $\widehat{V}_{\text{eff}}$ reflect the combined effects of the hydrodynamics of the buffer and the orthogonal electrical field applied to the system, under the assumptions stated, on the macrotransport parameters of the system. Both the characteristics of the electrical and hydrodynamic fields are included in these equations. In addition, geometrical dimensions and geometrical scaling for the electrical field (long channel approximation) and hydrodynamics (lubrication approximation) have been incorporated in this formulation.

Finally, by replacing the expressions of the variables identified in equations (31) & (32) and completing the spatial averaging indicated, the following analytical functions of the dimensionless effective parameters, θ and $\widehat{V}_{\text{eff}}$, are found:

$$\theta = \frac{-4\widehat{h}(\widehat{x})^2\left(360z\Omega\cosh\left(z\Omega/2\right) + z^4\Omega^4\sinh\left(z\Omega/2\right) - 60z^2\Omega^2\sinh\left(z\Omega/2\right) - 720\sinh\left(z\Omega/2\right)\right)}{5z^6\Omega^6\sinh\left(z\Omega/2\right)}, \tag{37}$$

$$\widehat{V}_{\text{eff}} = \frac{6\left(-2\sinh\left(z\Omega/2\right) + z\Omega\cosh\left(z\Omega/2\right)\right)}{z^2\Omega^2\sinh\left(z\Omega/2\right)}. \tag{38}$$

It can be observed that the above expression for θ is an explicit function of the line, $\widehat{h}(\widehat{x})$, representing the walls of the diverging capillary as well as the cation valence, z, and the dimensionless applied orthogonal electric field, Ω, whereas the $\widehat{V}_{\text{eff}}$ expression is not a function of $\widehat{h}(\widehat{x})$. This observation is useful to study the roles that these parameters play on the universal dispersion and effective velocity. This analysis is performed below.

7. Asymptotic Solutions: Validation of the Results for the Effective Transport Coefficients

Based on the equation for the effective dispersion coefficient, see Equation (37) (As $z\Omega$ and α approach zero, the limit of θ is -2/105, the Taylor-Aris result for purely Poiseuille flow (see Probstein [4]).), the following relation can be written:

$$\theta(\alpha) = \widehat{h}(\widehat{x})^2 \cdot \theta^0, \tag{39}$$

where

$$\theta^0 = \frac{-4\left(360z\Omega\cosh\left(z\Omega/2\right) + z^4\Omega^4\sinh\left(z\Omega/2\right) - 60z^2\Omega^2\sinh\left(z\Omega/2\right) - 720\sinh\left(z\Omega/2\right)\right)}{5z^6\Omega^6\sinh\left(z\Omega/2\right)}. \tag{40}$$

Alternatively, Equation (40) can be written as

$$\theta^0 = \frac{-4\cdot\left(\Omega^4 - 60\Omega^2 - 720\right)\cdot\left(e^{\Omega} - 1\right) + 360\cdot\Omega\cdot\left(e^{\Omega} + 1\right)}{5\cdot\Omega^6\cdot\left(e^{\Omega} - 1\right)}. \tag{41}$$

It is clear that for the case of $\alpha = 0$, the relation reduces to the equation published by Oyanader and Arce [8]. In short, the effective coefficient reproduces the asymptotic value for the strait pore geometry. In addition, equation (38) (Please note that as $z\Omega$ approaches zero, the limit of $\widehat{V}_{\text{eff}}$ is unity.) can be written in the exponential form as the following:

$$\widehat{V}_{\text{eff}} = \frac{12\cdot\left(1 - e^{\Omega}\right) + 6\cdot\Omega\cdot\left(1 + e^{\Omega}\right)}{\Omega^2\cdot\left(e^{\Omega} - 1\right)}. \tag{42}$$

By comparison, Equation (42) with Equation (22b) from Oyanader and Arce [49] leads to the conclusion that they are exactly the same. Again, the straight-pore geometry result is reproduced for the asymptotic case of $\alpha = 0$. In conclusion, the fact that the limiting case for the straight-pore domain ($\alpha = 0$) coincides exactly with the results reported in the previous work indicates a validating case for the general situation at hand in this contribution, i.e., $\alpha \neq 0$.

8. Parametric Analysis of the Effective Transport Coefficients and Discussion

This section includes graphical illustrations for the analytical results found in the previous section of this contribution. These illustrations show the dependence of the effective parameters, θ, the universal dispersion, and $\widehat{V}_{\text{eff}}$,

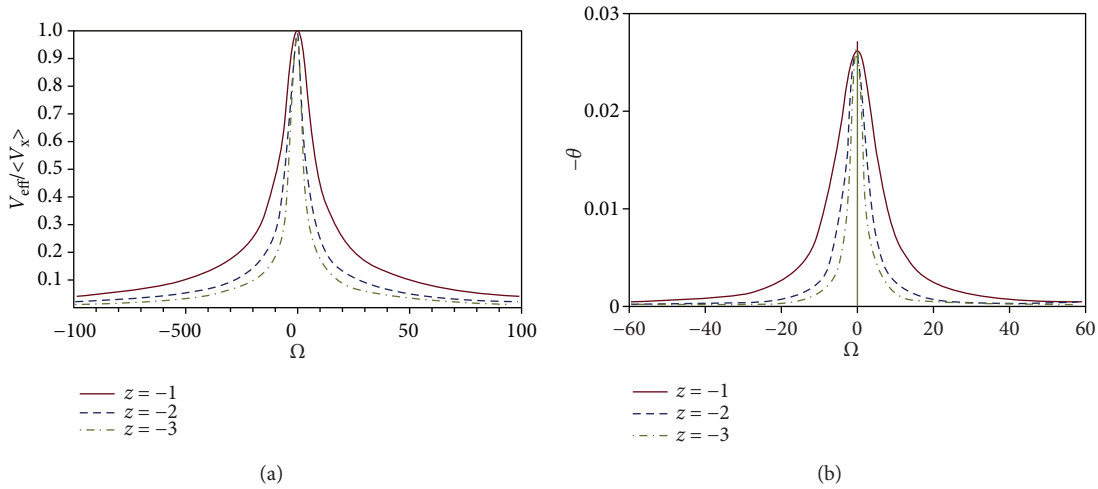

Figure 2: (a) Effective velocity as a function of the dimensionless orthogonal field, Ω, for various values of the valence, z. (b) Universal dispersion coefficient plotted against the dimensionless orthogonal field, Ω, and $\widehat{x} = 0.5$, $\alpha = 5$, and $\gamma = 0.5$ for varying values of valence, z.

the nondimensional effective mobility, on the geometrical and physicochemical properties of the system. Specifically, in this section, the direct dependence of these two effective transport coefficients with key parameters dictating the geometry of the pore (i.e. γ, the aspect ratio, α, the angle of divergence, and $\widehat{x}$, the dimensionless axial position), as well as physicochemical parameters such as the molecular charges (z_j), and the applied nondimensional orthogonal electrical field, Ω, will de illustrated. However, the importance of the role that these parameters could play on determining the optimal separation time of biomacromolecules will be discussed in detail in Section 7.

Figures 2(a) and 2(b) show the influence of the molecular charges on the effective mobility coefficient and on the universal dispersion, with respect to the applied orthogonal field, Ω, respectively. In the plots, the values for Ω have been obtained for the values of the parameters within the range selected previously by Sauer [6]. Figure 2(a) shows the variation of the effective transport coefficient, $\widehat{V}_{\text{eff}}$, with respect to Ω, the dimensionless applied orthogonal electrical field, for various values of the valence, z. It can be observed that as the magnitude of the electrical field increases, the effective velocity asymptotes to a value of zero, whereas, when Ω tends to a value of zero (i.e., no applied orthogonal electrical field), the effective velocity approaches a value of one. These results imply that as the magnitude of the electrical field increases, the molecules within the system will approach the velocities of the two pore walls (i.e., zero). The degree to which the particles approach the walls can also be deduced from Figure 2(b) as shown by the effect of the valence.

In Figure 2(b), the universal dispersion coefficient is plotted as a function of Ω for different values of valence, z, and selected values of $\alpha = 5$, $\gamma = 0.05$, and $\widehat{\mathrm{x}} = 0.5$. It can be seen that a maximum in dispersion is reached when the applied electrical field approaches zero, and the dispersion approaches a value of zero as the magnitude of the applied electrical field increases. As the magnitude of the charges increases (negatively), the shape of the bell curve of the dispersion gets narrower implying that a given value of the function θ can be obtained for smaller values of the applied orthogonal filed, Ω.

Figures 3(a) and 3(b) represent the impact on the universal dispersion, θ, of two geometrical parameters, the nondimensional axial position within the pore domain, x, and the shape factor (γ) of such a pore domain. Clearly, positions closer to the pore entrance ($x = 0$) show less values in the magnitude of the parameter ($-\theta$) for values of $\alpha = 5$, $z = -1$, and $\gamma = 0.05$. This behavior shows a decrease in the nondimensional effective diffusion coefficient, D_{eff}/D. Figure 3(b) shows the parametric effect of the shape factor, γ, for the same value of the divergence angle and molecular charges as before and at $x = .5$. As the values of the shape factor decreases (longer pore domains), the values of ($-\theta$) increases implying an increase in the nondimensional effective diffusion coefficient, D_{eff}/D, related to the pore domain.

Figures 4 illustrates the impact of the divergence angle, α, on the universal dispersion coefficient, θ, with respect to the nondimensional applied orthogonal field, Ω, parametrically, for different values of the divergence angle, α, that have been selected; i.e., $\alpha = 0$, $\alpha = 5$, $\alpha = 10$, and $\alpha = 15$. All the values of the divergence angle have been selected such as less than $\alpha = 20$ to comply with the restriction of the lubrication approximation. Values of the shape factor are kept at $\gamma = .05$ and at a position $x = .5$ inside the pore domain with a value of the molecular charge or valence of $z = -1$. The general trends are that (absolute) values of the dispersion coefficient decreases when the values of the divergent angle also decrease. This implies that the effective dispersion decreases as the pore tends to be more strait in their shape. The results are consistent (qualitatively) with those published by Simhadri [14]. This type of results is a clear indication of the dramatic role played by the geometry of the domain on the values of the effective transport coefficients that control the motion of the macromolecules inside the pores of the gel matrix.

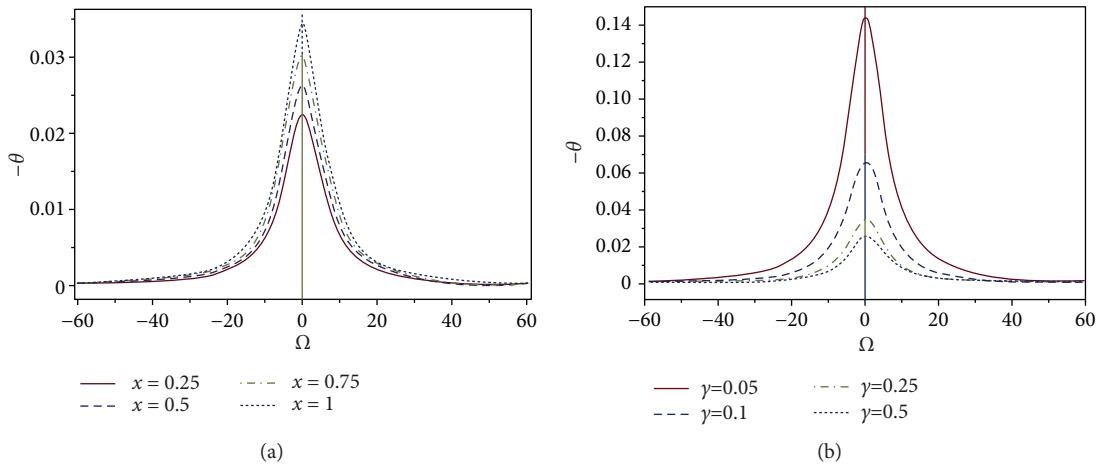

Figure 3: (a) Universal dispersion coefficient plotted against the dimensionless orthogonal field, Ω, and $\widehat{x} = 0.5$, $z = -1$, and $\gamma = 0.5$ for various values of the dimensionless axial position, $\widehat{x}$. (b) Universal dispersion coefficient plotted against the dimensionless orthogonal field, Ω, and $\widehat{x} = 0.5$, $z = -1$, and $\alpha = 5$ for various values of the aspect ratio, γ.

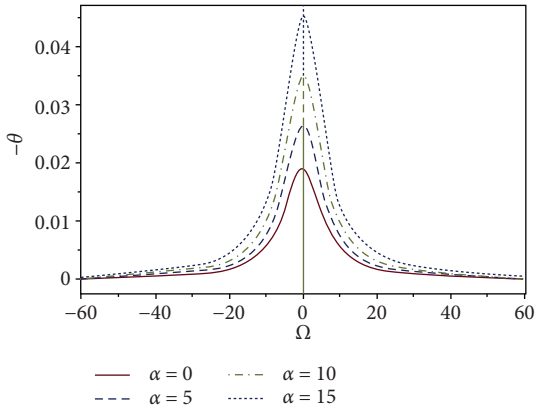

Figure 4: Universal dispersion coefficient plotted against the dimensionless orthogonal field, Ω, and $\widehat{x} = 0.5$, $z = -1$, and $\gamma = 0.5$ for various values of the angle of divergence, α.

9. Practical Implications of the Results: Optimal Time of Separation

The impact on the practical aspects of the results, obtained in Section 4 and illustrated in Section 6, deserves illustration to gain a better understanding of the role played by the irregular shape of the pore geometry on the electrophoresis; and an attempt to illustrate some of their useful implications for the separation of biomacromolecules is included in this section. The focus of this discussion is on the potential effects of the orthogonal electrical field and the (axially varying) morphology of the capillary, on the time required for optimal separation of two solutes with given physicochemical properties. In this regard, one of the most difficult examples of separation is the case of two species of approximately equal molecular diffusivities. This specific case is an ideal candidate for applying orthogonal electric fields in order to take advantage of other physicochemical properties (i.e., electrophoretic mobility, μ, and cation valence, z) or the morphology of the gel. Sauer and collaborators [6] and Oyanader and Arce [8] calculated the time required to achieve an "optimal" separation (resolution of two) to illustrate practical applications of applied electric fields. Following this approach, analytical expressions for effective transport parameters in order to estimate the optimal time of separation of two hypothetical species based on various parameters, including the angle of divergence, α, aspect ratio, γ, and dimensionless axial position, $\widehat{x}$, that characterize the pore geometry under analysis, have been computed. In addition, since the equations predicting the effective parameters show a direct dependence on the orthogonal electrical field, Ω, the effect of this parameter on the optimal time, τ_{op}, for the separation of biomacromolecules is determined.

Applying the definition of the dimensionless orthogonal electric field (please see equation (32)), $\Omega \equiv K_2 \mu / D$, to two hypothetical species with very similar molecular diffusivity values, but different electrophoretic mobilities, the following expression can be utilized to relate the effects of Ω between the two species:

$$\Omega_B = \left(\frac{\mu_B}{\mu_A}\right) \Omega_A, \tag{43}$$

where the term μ_B/μ_A has been defined as the electrophoretic mobility ratio. Equation (43) indicates that for a given value of applied electric field K_2 to the system, species B is affected by a dimensionless electric field Ω_B proportional to the electric field affecting species A, Ω_A, by a factor of the mobility ratio μ_B/μ_A. Another important parameter for analysis of the optimal separation time variation with Ω is the cation valence ratio. For two species, similarly to equation (43), we have defined the following valence ratio: z_B/z_A.

The time of separation of two species, for a resolution of 2, has been defined by the following expression (see Sauer et al. [6]):

$$\tau_{op} = \left[\frac{\sqrt{D_{\text{eff }A}/D_A} + \sqrt{D_{\text{eff }B}/D_B}}{\widehat{V}_{\text{eff }A} - \widehat{V}_{\text{eff }B}}\right]^2, \tag{44}$$

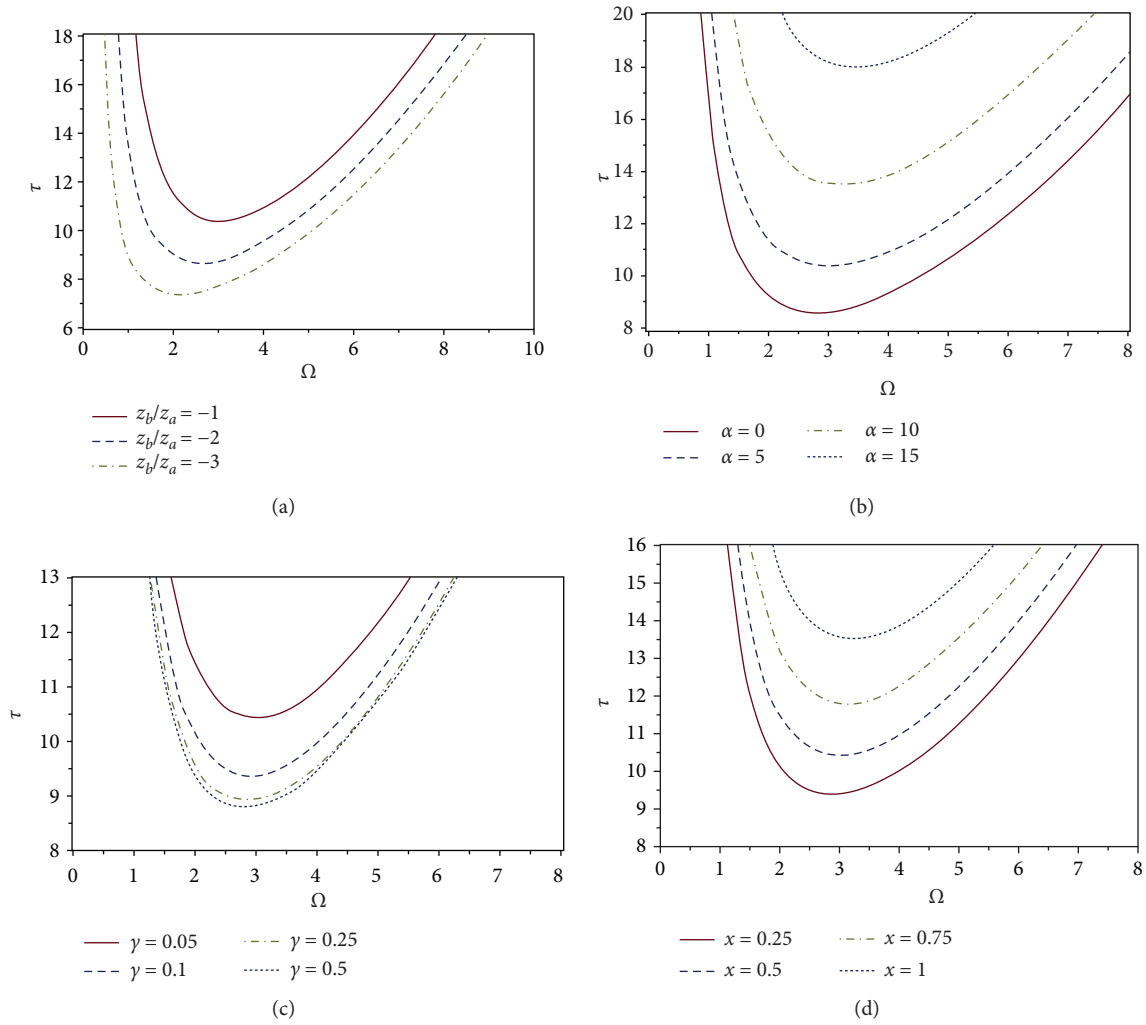

Figure 5: (a) Optimal time of separation predicted for a resolution with a value of two in a diverging pore with orthogonal applied electrical field ($\Omega_A = \Omega$): Pe = 2, $\gamma = 0.05$, $\hat{x} = 0.5$, $\alpha = 5$, $\mu_B/\mu_A = 5$, and different valence ratio, z_B/z_A, values. (b) Optimal time of separation predicted for a resolution with a value of two in a diverging pore with orthogonal applied electrical field ($\Omega_A = \Omega$): Pe = 2, $\gamma = 0.05$, $\hat{x} = 0.5$, $\mu_B/\mu_A = 5$, $z_B/z_A = 2$, and different angles of divergence, α. (c) Optimal time of separation predicted for a resolution with a value of two in a diverging pore with orthogonal applied electrical field ($\Omega_A = \Omega$): Pe = 2, $\gamma = 0.05$, $\hat{x} = 0.5$, $\mu_B/\mu_A = 5$, $z_B/z_A = 2$, and different aspect ratio, γ, values. (d) Optimal time of separation predicted for a resolution with a value of two in a diverging pore with orthogonal applied electrical field ($\Omega_A = \Omega$): Pe = 2, $\gamma = 0.05$, $\hat{x} = 0.5$, $\mu_B/\mu_A = 5$, $z_B/z_A = 2$, for various dimensionless axial position, $\hat{x}$, values.

where all the terms have been previously identified and/or defined (see equations (33) and (34)) as functions of the dimensionless orthogonal field, Ω, and the subscripts indicate the species for which the term must be computed, either using Ω_A or Ω_B. Please note that D_{eff}/D and $\hat{V}_{\text{eff}}$ are functions of the valence of each cation species, so that z_A and z_B may be specified to compute the optimal separation time,τ_{op}. Furthermore, the combination of equations (43) and (44) can be used to analyze the separation process under electric field stress.

Figures 5(a)–5(d) show the (optimal) separation time, τ_{op}, as a function of the nondimensional orthogonal field, Ω_A, taking species A as the reference. In particular, Figure 5(a) presents τ_{op} as a function of Ω_A for different values of the valence ratio, z_B/z_A, and Figure 5(b) shows the same variables for different values of the angle of divergence, α, for fixed values of the other parameters (i.e., mobility ratio, valence ratio, aspect ratio, and dimensionless axial position). Figures 5(c) & 5(d) show the same function for different γ and dimensionless axial position values,$\hat{x}$, respectively. It can be seen from Figure 5(a) that a minimum optimal separation time, τ_{op}, exists for values of Ω_A. This minimum is further influenced by the value of the valence ratio, z_B/z_A of the two species, A and B. It is evident that as z_B/z_A increases, the time for separation decreases, due to the increase in the difference in susceptibility of the two species to the applied orthogonal electrical field. Therefore, if the two species have vastly different charges, or valences, the model predictions indicate that they will be easier to separate under the action of an orthogonal electrical field.

As can be observed from Figure 5(b), optimal separation times decrease with decreasing values of the angle of

divergence of the pore, α. In particular, for $\alpha = 0$, the optimal separation time is much lower than for $\alpha = 10$ or $\alpha = 15$ (Although the lubrication approximation limits the validity of the approach to small angles (less than 20°), computational simulations show that the most dramatic changes for the system's behavior occur within the range of 0°-20° (Simhadri et al. [14]).). This result implies that a straight pore will create a better separation than a pore with a varying axial cross section will, since there will be less mixing of the two species. It is evident from Figure 5(c) that as the aspect ratio, γ, increases, the optimal separation time decreases. A large value of γ implies that the pore is shorter than it is long, whereas a small value of γ means that the pore is long. Therefore, from Figure 4(c), a shorter pore will lead to a lower optimal separation time.

Lastly, Figure 5(d) illustrates the effect of the dimensionless axial position within the pore on the optimal separation time. It can be seen from this figure that for low values of $\widehat{x}$ (i.e., near the entrance of the pore), the optimal separation time decreases, and for high values of $\widehat{x}$ (i.e., near the exit of the pore), the optimal separation time increases. This is due (most likely) to the fact that near the entrance of the pore (low values of $\widehat{x}$), the species do not have enough time to mix and therefore will be significantly easier to separate with an applied orthogonal electrical field, than if they were at a position near the exit of the pore. From the results discussed in this section and within the assumptions of the analysis, it can be concluded that a straight, short capillary will produce a lower optimal separation time. This result is indicative of the potentially important interplay of scaling, capillary morphology, and the direction of the applied field in order to improve separation. Moreover, an optimal operation requires the consideration (most likely) of all of them together as opposed to the "in isolation" fashion customarily used. The prediction of the optimal time of separation is consistent with those reported by Simhadri et al. [14] and with experimental evidences reported by Thompson et al. [17]. A complete scaling analysis and a quantitative comparison are outside the scope of this contribution; however, it will be the subject matter of the future communication.

10. Summary and Concluding Remarks

For the case of gel electrophoresis of charged solutes in gels modeled as a pore bundle, with uniform pore of an irregular shape, the results reported here clearly show the explicit dependence of the effective diffusivity and the optimal separation time (within the assumptions of the analysis) on the orthogonal field as well as the geometrical parameters of the capillary, including the aspect ratio, the axial position, and the angle of divergence. The case of electrophoresis separation of two solutes under an applied, orthogonal, and constant field is analyzed for a diverging pore cavity. These types of geometrical voids are hypothesized as possibly being housed in a nanocomposite gel [17, 53]. Expressions for the *effective* system parameters have been derived by using the EKHD method (Tijaro-Rojas et al. [17]) without actually solving for the concentration profiles. Taking advantage of this methodology, constitutive equations of the effective, or alternatively "macrotransport" transport parameters, i.e., the effective diffusivity or, even more general, the universal dispersion parameter, and the effective velocity, are obtained as a function of fundamental variables such as the magnitude of the electrical field, cation valence, angle of divergence, aspect ratio, and axial position (This type of functionality is, in general, tied to the characteristics of the electrical and hydrodynamic fields and our claims are by no means valid outside the specific assumptions and characteristics used in this analysis. The variation of the effective transport parameters with the location is consistent with analysis conducted for other geometries (see Nagarkar et al. [54]).). These functions are useful in identifying conditions for minimum values of the optimal separation time for two solutes. The potential benefits of the predicting equations for the design of optimal conditions for the electrophoresis separations of biomacromolecules are clearly shown. For a gel with diverging pore geometry, and to the best of our knowledge, these analytical results are not available in the current literature and it is the hope of the authors that they contribute to the better understanding of the fundamental role of morphology and the orthogonal field in electrophoretic separations with relevance for gels, with a modified morphology, microcapillary electrophoresis, and other similar cases.

Finally, and since the EKHD method uses concepts from continuum mechanics approaches, the results and observations of this contribution (most likely) will be also valid for the microchannel or microcapillary scales in separation devices such as microfluidics. However, continuum mechanics approaches have been validated for the nanoscale in contributions reported in the literature. For example, Conlisk [55] conducted an analysis comparing the validity of the Debye-Hückel approximation in microchannels (i.e., channel height is greater than electrical double-layer thickness) and nanochannels (i.e., channel height is on the order of the electrical double-layer thickness). The results using the continuum approach compare well with experimental data for rectangular channels. On the other hand, it was reported that the continuum approach is not valid for nanochannels with a height of 6 nm or less. However, for most separations conducted in nanochannels, the height is at least 10 nm; therefore, the continuum assumptions should be valid. We believe that the results presented here could be a very useful first approximation for understanding the role of the morphology of the separation media beyond the microscopic scale and, possible, give a qualitative idea at behaviors of the media also valid for smaller scales.

Disclosure

Jennifer A. Pascal's present address is Department of Chemical and Biomolecular Engineering, University of Connecticut, USA. Preliminary versions of the results were presented at the American Electrophoresis Society (AES) Annual Meetings.

Conflicts of Interest

The authors declare that they have no conflicts of interest.

Acknowledgments

The authors are indebted to helpful discussions with Dr. Sharon G. Sauer of the Rose-Hulman Institute of Technology, Terre-Hautte, IN, and Dr. Y. Liu of the Department of Mathematics, TTU. Jennifer Pascal is grateful for a Diversity Fellowship from the Office of Research and Graduate Studies at Tennessee Technological University.

References

[1] H. Brenner and D. Edwards, *Macrotransport Processes*, Butterworth-Heinemann Series in Chemical Engineering, 1993.

[2] W. G. Gray, "A derivation of the equations for multi-phase transport," *Chemical Engineering Science*, vol. 30, no. 2, pp. 229–233, 1975.

[3] J. Pascal, R. O'Hara, M. Oyanader, and P. E. Arce, "Optimal separation times for electrical field flow fractionation with Couette flows," *Electrophoresis*, vol. 29, no. 20, pp. 4238–4246, 2008.

[4] R. Probstein, *An Introduction to Physicochemical Hydrodynamics*, John Wiley, New York, NY, USA, 1991.

[5] J. H. Masliyah and S. Bhattacharjee, *Electrokinetic and Colloid Transport Phenomena*, John Wiley and Sons Inc., Hoboken, NJ, USA, 2006.

[6] S. G. Sauer, B. R. Locke, and P. Arce, "Effects of axial and orthogonal applied electric fields on solute transport in Poiseuille flows. An area averaging approach," *Industrial & Engineering Chemistry Research*, vol. 34, no. 3, pp. 886–894, 1995.

[7] C. S. Lee, C.-T. Wu, T. Lopes, and B. Patel, "Analysis of separation efficiency in capillary electrophoresis with direct control of electroosmosis by using an external electric field," *Journal of Chromatography A*, vol. 559, no. 1-2, pp. 133–140, 1991.

[8] M. A. Oyanader and P. Arce, "Role of geometrical dimensions in electrophoresis applications with orthogonal fields," *Electrophoresis*, vol. 26, no. 15, pp. 2857–2866, 2005.

[9] R. C. Wu and K. D. Papadopoulos, "Electroosmotic flow through porous media: cylindrical and annular models," *Colloids and Surfaces A: Physicochemical and Engineering Aspects*, vol. 161, no. 3, pp. 469–476, 2000.

[10] J. Pascal, M. Oyanader, and P. Arce, "Effect of capillary geometry on predicting electroosmotic volumetric flowrates in porous or fibrous media," *Journal of Colloid and Interface Science*, vol. 378, no. 1, pp. 241–250, 2012.

[11] S. Trinh, B. R. Locke, and P. Arce, "Diffusive–convective and diffusive–electroconvective transport in non-uniform channels with application to macromolecular separations," *Separation and Purification Technology*, vol. 15, no. 3, pp. 255–269, 1999.

[12] S. Trinh, P. Arce, and B. R. Locke, "Effective diffusivities of point-like molecules in isotropic porous media by Monte Carlo simulation," *Transport in Porous Media*, vol. 38, no. 3, pp. 241–259, 2000.

[13] S. Trinh, B. R. Locke, and P. Arce, "Effective diffusivity tensors of point-like molecules in anisotropic porous media by Monte Carlo simulation," *Transport in Porous Media*, vol. 47, no. 3, pp. 279–293, 2002.

[14] J. J. Simhadri, H. A. Stretz, M. A. Oyanader, and P. E. Arce, "Assessing performance of irregular microvoids in electrophoresis separations," *Industrial & Engineering Chemistry Research*, vol. 54, no. 42, pp. 10434–10441, 2015.

[15] J. Pascal, R. Tíjaro-Rojas, M. A. Oyanader, and P. E. Arce, "The acquisition and transfer of knowledge of electrokinetic-hydrodynamics (EKHD) fundamentals: an introductory graduate-level course," *European Journal of Engineering Education*, vol. 42, no. 5, pp. 493–512, 2016.

[16] P. E. Arce, N. E. Allred, S. Blanton, and J. R. Sanders, "Electrokinetic-hydrodyanmics (EKHD): an efficient framework for learning electrokinetics," in *EREM 2017 Proceedings*, Concordia University, Montreal, Canada, August 2017.

[17] J. W. Thompson, H. A. Stretz, P. E. Arce, H. Gao, H. J. Ploehn, and J. He, "Effect of magnetization on the gel structure and protein electrophoresis in polyacrylamide hydrogel nanocomposites," *Journal of Applied Polymer Science*, vol. 126, no. 5, pp. 1600–1612, 2012.

[18] G. Huang, Y. Zhang, J. Ouyang, W. R. G. Baeyens, and J. R. Delanghe, "Application of carbon nanotube-matrix assistant native polyacrylamide gel electrophoresis to the separation of apolipoprotein A-I and complement C3," *Analytica Chimica Acta*, vol. 557, no. 1-2, pp. 137–145, 2006.

[19] N. C. Stellwagen, "Electrophoresis of DNA in agarose gels, polyacrylamide gels and in free solution," *Electrophoresis*, vol. 30, Supplement 1, pp. S188–S195, 2009.

[20] M. E. Byrne and V. Salian, "Molecular imprinting within hydrogels II: progress and analysis of the field," *International Journal of Pharmaceutics*, vol. 364, no. 2, pp. 188–212, 2008.

[21] J. R. Dharia, R. Pill, D. van Winkle, B. R. Locke, and P. E. Arce, "Preparation and characterization of polyacrylamide gels containing micro channels," in *FLACS (Florida Section of ACS) Annual Meeting*, Orlando, FL, USA, May 1994.

[22] R. L. Rill, B. R. Locke, Y. Liu, J. Dharia, and D. van Winkle, "Protein electrophoresis in polyacrylamide gels with templated pores," *Electrophoresis*, vol. 17, no. 8, pp. 1304–1312, 1996.

[23] J. W. Thompson, H. Stretz, and P. Arce, "Thermoresponsive Micrcoparticel Gels Eletrophoresis Poly-n-Isopropylacrylamide Microparticle PAGE," in *ACS National Conference*, New Orleans, LA, USA, 2008.

[24] M. V. Carranza-Oropeza, A. W. Sherrill, J. R. Sanders, P. E. Arce, and R. Giudici, "Performance assessment of protein electrophoresis by using polyacrylamide hydrogel with porous structure modified with SDS micelles as template," *Journal of Applied Polymer Science*, vol. 133, no. 40, 2016.

[25] J. Simhadri, H. Stretz, M. Oyanader, and P. Arce, "Morphology of Nanocomposite and Template Gels and its Role in the Separation of Biomolecules: A Review," *I&EC Research*, vol. 49, no. 23, pp. 12104–12110, 2010.

[26] J. Texter, "Templating hydrogels," *Colloid and Polymer Science*, vol. 287, no. 3, pp. 313–321, 2009.

[27] M. Horner, P. Arce, and B. R. Locke, "Convective-diffusive transport and reaction in arterial stenoses using lubrication and area-averaging methods," *Industrial and Engineering Chemistry Research*, vol. 34, no. 10, pp. 3426–3436, 1995.

[28] E. H. Cwirko and R. G. Carbonell, "Transport of electrolytes in charged pores: analysis using the method of spatial averaging," *Journal of Colloid and Interface Science*, vol. 129, no. 2, pp. 513–531, 1989.

[29] M. A. Paine, R. G. Carbonell, and S. Whitaker, "Dispersion in pulsed systems—I: heterogenous reaction and reversible adsorption in capillary tubes," *Chemical Engineering Science*, vol. 38, no. 11, pp. 1781–1793, 1983.

[30] J. C. Slattery, *Momentum, Energy and Mass Transfer in Continua*, Krieger, New York, NY, USA, 1981.

[31] S. Whitaker, "The Spatial Averaging Theorem Revisited," *Chemical Engineering Science*, vol. 40, p. 1387, 1985.

[32] F. Zanotti and R. G. Carbonell, "Development of transport equations for multiphase system—I: general development for two phase system," *Chemical Engineering Science*, vol. 39, no. 2, pp. 263–278, 1984.

[33] F. Zanotti and R. G. Carbonell, "Development of transport equations for multiphase systems—II: application to one-dimensional axi-symmetric flows of two phases," *Chemical Engineering Science*, vol. 39, no. 2, pp. 279–297, 1984.

[34] F. Zanotti and R. G. Carbonell, "Development of transport equations for multiphase systems—III: application to heat transfer in packed beds," *Chemical Engineering Science*, vol. 39, no. 2, pp. 299–311, 1984.

[35] X. Xuan, B. Xu, and D. Li, "Accelerated particle electrophoretic motion and separation in converging–diverging microchannels," *Analytical Chemistry*, vol. 77, no. 14, pp. 4323–4328, 2005.

[36] S. Ghosal, "Electrophoresis of a polyelectrolyte through a nanopore," *Physical Review E*, vol. 74, no. 4, article 041901, 2006.

[37] S. Ghosal, "Lubrication theory for electro-osmotic flow in a microfluidic channel of slowly varying cross-section and wall charge," *Journal of Fluid Mechanics*, vol. 459, pp. 103–128, 2002.

[38] D. Ross, C. F. Ivory, L. E. Locascio, and K. E. Van Cott, "Peak compression and resolution for electrophoretic separations in diverging microchannels," *Electrophoresis*, vol. 25, no. 21-22, pp. 3694–3704, 2004.

[39] E. Yariv and K. D. Dorfman, "Electrophoretic transport through channels of periodically varying cross section," *Physics of Fluids*, vol. 19, no. 3, article 037101, 2007.

[40] C. Eringen and G. A. Maugin, Eds., *Electrohydrodynamics of Continuum II: Fluids and Complex Media*, Springer-Verlag, Berlin, 1990.

[41] P. C. Hiemenz, *Principles of Colloid and Surface Chemistry*, Dekker, New York, NY, USA, 2nd edition, 1986.

[42] R. J. Hunter, *Foundations of Colloid Science, Vols. I and II*, Clarendon Press, Oxford, 1989.

[43] L. J. Gajdos and H. Brenner, "Field-flow fractionation: extensions to nonspherical particles and wall effects," *Separation Science and Technology*, vol. 13, no. 3, pp. 215–240, 1978.

[44] C. Heller, T. Duke, and J. L. Viovy, "Electrophoretic mobility of DNA in gels. II. Systematic experimental study in agarose gels," *Biopolymers*, vol. 34, no. 2, pp. 249–259, 1994.

[45] F. Baldessari and J. G. Santiago, "Electrophoresis in nanochannels: brief review and speculation," *Journal of Nanobiotechnology*, vol. 4, no. 1, p. 12, 2006.

[46] J. Simhadri, "Design and Optimization of Separation Performance in Porous Materials," *PhD Thesis*, Tennessee Technological University, Cookeville, TN, USA, 2013.

[47] P. E. Arce, M. Oyanader, and S. Whitaker, "The catalytic pellet: a rich learning environment for up-scaling," *Journal of Chemical Engineering Education*, vol. 41, no. 3, pp. 187–194, 2007.

[48] J. Simhadri, H. Stretz, and P. E. Arce, "Role of channel morphology in electrophoresis separation: an optimization by differential evolution," *Brazilian Journal of Chemical Engineering*, vol. 33, no. 1, pp. 123–131, 2016.

[49] R. B. Bird, W. Stewart, and E. N. Lightfoot, *Transport Phenomena*, John Wiley, New York, NY, USA, 2 Edition edition, 2002.

[50] S. Whitaker, *Fundamentals Principles of Heat Transfer*, Krieger Publisher, Melbourne, FL USA, 1983.

[51] W. Deen, *Analysis of Transport Phenomena (Topics in Chemical Engineering)*, Oxford University Press, USA, 1998.

[52] M. Denn, *Process Fluid Mechanics*, Prentice Hall, 1979.

[53] J. Pascal, P. E.. Arce, M. Oyanader, and S. Sauer, *Electrokinetic-Hydrodynamics: A Much-Needed Framework for Applied Electrical Field Sensitive Technologies*, vol. 14, American Electrophoresis Society, Newsletter, 2009.

[54] A. S. Nagarkar, P. Arce, and B. R. Locke, "Convective-diffusive mass transfer with chemical reaction in squeezing flows," *Industrial & Engineering Chemistry Research*, vol. 35, no. 4, pp. 1012–1023, 1996.

[55] A. T. Conlisk, "The Debye-Hückel approximation: its use in describing electroosmotic flow in micro- and nanochannels," *Electrophoresis*, vol. 26, no. 10, pp. 1896–1912, 2005.

[56] K. Haraguchi, T. Takehisa, and S. Fan, "Effects of clay content on the properties of nanocomposite hydrogels composed of poly (N-isopropylacrylamide) and clay," *Macromolecules*, vol. 35, no. 27, pp. 10162–10171, 2002.